Published in final edited form as:
Cell Metab. 2011 August 3; 14(2): 184–195. doi:10.1016/j.cmet.2011.06.009.

Deletion of the Mammalian *INDY* Homologue Mimics Aspects of Dietary Restriction and Protects Against Adiposity and Insulin Resistance in Mice

Andreas L. Birkenfeld[1,2], **Hui-Young Lee**[1], **Fitsum Guebre-Egziabher**[1], **Tiago C. Alves**[1], **Michael J. Jurczak**[1], **Francois R. Jornayvaz**[1], **Dongyang Zhang**[1], **Jennifer J. Hsiao**[1], **Alejandro Martin-Montalvo**[3], **Antje Fischer-Rosinsky**[2], **Joachim Spranger**[2], **Andreas F. Pfeiffer**[2], **Jens Jordan**[4], **Martin F. Fromm**[5], **Jörg König**[5], **Stefanie Lieske**[2], **Christopher M. Carmean**[1], **David W. Frederick**[1], **Dirk Weismann**[1], **Felix Knauf**[1], **Pablo M. Irusta**[6], **Rafael De Cabo**[3], **Stephen L. Helfand**[7], **Varman T. Samuel**[1], and **Gerald I. Shulman**[1,‡]

[1]Howard Hughes Medical Institute and the Departments of Internal Medicine and Cellular & Molecular Physiology Yale School of Medicine, New Haven, CT 06520, USA

[2]German Institute of Human Nutrition Potsdam-Rehbrücke, Germany and Charité - University School of Medicine, Berlin, Germany

[3]Laboratory of Experimental Gerontology, National Institute on Aging, Baltimore, MD 21224, USA

[4]Institute of Clinical Pharmacology, Hannover School of Medicine, Hannover, Germany

[5]Institute of Experimental and Clinical Pharmacology and Toxicology, Friedrich-Alexander-University, Erlangen-Nürnberg, Germany

[6]Department of Human Science, Georgetown University, Washington, D.C. 20057, USA

[7]Department of Molecular Biology, Cell Biology and Biochemistry, Brown University, Providence, RI 02912, USA

SUMMARY

Reduced expression of the *Indy (= **I** am **N**ot **D**ead, **Y**et)* gene in *D. melanogaster* and *C. elegans* prolongs life span, and in *D. melanogaster* augments mitochondrial biogenesis in a manner akin to caloric restriction. However, the cellular mechanism by which *Indy* does this is unknown. Here, we report on the knockout-mouse model of the mammalian *Indy* (*mIndy*) homologue, *SLC13A5*. Deletion of *mIndy* in mice (mINDY$^{-/-}$ mice) reduces hepatocellular ATP/ADP ratio, activates hepatic AMPK, induces PGC-1α, inhibits ACC-2, and reduces SREBP-1c levels. This signaling network promotes hepatic mitochondrial biogenesis, lipid oxidation, and energy expenditure and attenuates hepatic *de novo* lipogenesis. Together, these traits protect mINDY$^{-/-}$ mice from the adiposity and insulin resistance that evolve with high-fat feeding and aging. Our studies demonstrate a profound effect of *mIndy* on mammalian energy metabolism and suggest that mINDY might be a therapeutic target for the treatment of obesity and type 2 diabetes.

‡To whom correspondence should be addressed. gerald.shulman@yale.edu .

INTRODUCTION

Energy balance and insulin action are both closely related to life span. Whereas caloric excess leads to obesity, insulin resistance and increased mortality, caloric restriction reduces adiposity and increases lipid oxidation, insulin sensitivity, and mitochondrial biogenesis. In addition, caloric restriction reverses obesity, type 2 diabetes, delays aging, and prolongs life in many species, including primates (Hursting et al., 2003; Lopez-Lluch et al., 2006; Hunt et al., 2006; Fontana and Klein, 2007; Colman et al., 2009). Mediators of the beneficial effects of caloric restriction include decreased plasma concentrations of anabolic hormones and growth factors, i.e. insulin and insulin like growth factors (Fontana and Klein, 2007). Reduced expression of the *Indy* (for ***I*** am ***N***ot ***D***ead, ***Y***et) gene in *D. melanogaster* and *C. elegans* has been shown to promote longevity in a manner akin to caloric restriction, however the cellular mechanism by which reduced expression of *Indy* leads to increased survival is unknown (Rogina et al., 2000; Fei et al., 2004; Fei et al., 2003; Wang et al., 2009).

In *D. melanogaster*, *Indy* encodes a non-electrogenic dicarboxylate and citrate transporter (Knauf et al., 2002; Knauf et al., 2006) and it is mainly expressed in the fat body, mid gut, and oenocyte (Rogina et al., 2000), thus, the major organs of intermediary metabolism in flies. In mammals, the gene product of *SLC13A5*, the sodium-coupled citrate transporter NaCT (mINDY), shares the highest sequence and functional similarity with *D. melanogaster INDY* (Inoue et al., 2002a) and it is predominantly expressed in liver cells (Inoue et al., 2002b; Knauf et al., 2002; Knauf et al., 2006; Gopal et al., 2007).

In order to examine the effect that INDY might have on energy metabolism and insulin sensitivity in mammals we created a knockout mouse model (mINDY$^{-/-}$ mice) of the mammalian *Indy* homologue *SLC13A5 (mIndy)* and assessed the effect of *mIndy* deletion on energy homeostasis and energy storage *in vivo*. Furthermore, we assessed the impact of *mIndy* deletion on insulin action, in young, chow-fed mice, as well as after exposing them to two perturbations known to induce insulin resistance, specifically, high-fat feeding and aging.

RESULTS

Transport kinetics of mINDY

cDNA encoding mINDY was cloned and stably transfected into HEK293 cells. The uptake capacities of mINDY for the two substrates with the highest plasma concentrations, namely citrate and succinate, were analyzed. mINDY is a high capacity transporter for citrate at physiological concentrations (K_m=49±9 μM, V_{max}=3760±160 [pmol/(mg × min)]) (Figure 1A) and it transports succinate with an intermediate capacity (K_m=105±9 μM, V_{max}=443±20 [pmol/(mg × min)]) (Figure 1B).

Generation of mINDY$^{-/-}$ mice

mINDY$^{-/-}$ mice were generated as described in supplemental figures S1A-E. We performed Southern blot analysis for FloxP detection under stringent hybridization and washing conditions. The results shown in supplemental figure S1E clearly indicate that the digests obtained with BamH1 gave one single band for wild type and KO/+ genomic DNA samples (3.5kb) while the FloxP/+ genomic DNA samples showed the 3.5 kb band and a specific band of 1.76kb which correspond to the FloxP construction. The litters produced when heterozygous (KO/+) mINDY mice (mINDY$^{+/-}$) were bred, contained the expected ratio of *mIndy* wild-type (mINDY$^{+/+}$), mINDY$^{+/-}$ mice, and homozygous *mIndy* (mINDY$^{-/-}$) pups, indicating no substantial embryonic lethality. In wild-type mice, *Indy* mRNA expression was highest in liver, and low in white adipose tissue, brown adipose tissue, skeletal muscle,

small intestines and the pancreas (Figure 1C), confirming previous *mIndy* expression levels in rodents (Gopal et al., 2007), and humans (Nishimura and Naito, 2008). Liver *mIndy* mRNA expression was completely abolished in the INDY$^{-/-}$ mice and ~50% reduced in heterozygous mINDY$^{+/-}$ mice (Supplemental Figure S1D). Functional significance of differences in *mIndy* expression patterns in different organs and tissues was evaluated by comparing the uptake of [^{14}C]-citrate during an infusion study *in vivo* in mINDY$^{+/+}$ and mINDY$^{-/-}$ mice. In line with the highest expression of *mIndy* in liver, mINDY$^{-/-}$ mice showed a 20% reduction in hepatic citrate uptake (P=0.03), without significant differences in citrate uptake into skeletal muscle, and kidney (Figure 1D). [^{14}C]-citrate uptake in primary hepatocytes from mINDY$^{+/+}$ and mINDY$^{-/-}$ mice indicated a reduced citrate uptake by 36% into mINDY$^{-/-}$ primary hepatocytes (data not shown).

Expression of *SLC13A3*, another hepatic plasma membrane tri-/dicarboxylate transporter, was increased ~ 3fold in the liver of regular chow fed mINDY$^{-/-}$ mice, probably compensating for *mIndy*-loss. This compensatory increase was completely abolished when mice were fed a HFD (Supplemental Figure S2). *mIndy* expression did not change significantly with high fat feeding or aging in mice (data not shown). In accordance with reduced cellular citrate uptake, GC/MS plasma metabolite analysis revealed increased relative plasma citrate concentrations in the mINDY$^{-/-}$ mice, a trend for increased malate concentrations, and no changes in succinate and fumarate concentrations (Figure 1E).

Body weight and energy expenditure

Compared to mINDY$^{+/+}$ mice, body weights of mINDY$^{+/-}$ and mINDY$^{-/-}$ mice on a regular chow were 2% and 10% lower, respectively, at 4 weeks of age (Figure 2A). mINDY$^{-/-}$ mice showed an increasing difference in body weight compared to mINDY$^{+/+}$ mice with time (Figure 2A and 2B). The relative percentage of lean body mass and fat mass, as assessed by ^{1}H-MRS, did not differ between genotypes up to an age of 3 months (Supplemental Figure S3A). Body length of mINDY$^{+/-}$ and mINDY$^{-/-}$ mice at 3 months of age was 9.9±0.2cm and 9.9±0.1cm, respectively, and 10.2±0.1cm in mINDY$^{+/+}$ mice (Supplementary Figure S3B). Thus, loss of *mIndy* reduced overall growth. To determine the reasons, mice were studied in metabolic cages. Oxygen consumption (V_{O2}), carbon dioxide production (V_{CO2}) and energy expenditure were increased in the mINDY$^{-/-}$ mice (Supplemental Table S1). Because we observed a numerical increase in locomotor activity in the mINDY$^{-/-}$ mice, we also analyzed daytime energy expenditure and locomotor activity separately, which is the time when mice sleep and are typically inactive. During this time, a significant increase in energy expenditure was still observed, without a numerical difference in locomotor activity (Supplemental Figure S4A-D) These data suggest that differences in locomotor activity are likely due to a higher urge of the mINDY$^{-/-}$ mice to ingest their food, as evidenced by the sole increase in locomotor activity during the first 3-4h of food ingestion (Supplemental Figure S4A and S4B). These data exclude locomotor activity as the main cause of the increase in energy expenditure in the mINDY$^{-/-}$ mice.

Protection from nutritionally induced obesity

An increase in energy expenditure might limit weight gain on a HFD. Thus, we studied the effect of 6 weeks HFD (55% Kcal from fat) on body weight and whole body fat accumulation. Body weight was reduced by 17% in the mINDY$^{-/-}$ mice compared to mINDY$^{+/+}$ mice (Figure 3A), and the proportion of fat mass to body weight was markedly reduced (Figure 3B), while lean body mass was increased in mINDY$^{-/-}$ mice (Figure 3B). Energy expenditure was also increased in the mINDY$^{-/-}$ mice (Supplemental Table S1, and Supplemental Figure S4A and S4B). Basal plasma β-hydroxybutyrate, a marker of hepatic lipid oxidation, was increased by 18% and by 62% in the mINDY$^{+/-}$ mice and the mINDY$^{-/-}$ mice, respectively (Figure 3C). To further determine if this effect is specific to

liver tissue, we measured hepatic lipid oxidation in primary hepatocytes from mINDY$^{-/-}$ mice and mINDY$^{+/+}$ mice fed a HFD. Primary mINDY$^{-/-}$ hepatocytes showed an increased proportion of lipid oxidation compared to mINDY$^{+/+}$ hepatocytes by 32% (Figure 3D). Fittingly, mINDY$^{-/-}$ liver homogenate showed an increase in oxygen consumption by 23% (Figure 3E). Citrate can be converted to acetyl-CoA by ATP-citrate lyase and used for lipid generation. Reduced lipogenesis could contribute to reduced lipid accumulation. Consistent with this possibility we found that [^{14}C]-citrate incorporation into intracellular sterols and fatty acids was reduced by ~90% in primary mINDY$^{-/-}$ hepatocytes (Figure 3F). Together these data show that loss of *mIndy* reduces hepatic lipid generation from external citrate and induces hepatic lipid oxidation.

Protection from high fat diet induced hepatic steatosis

Reduced proportions of fat mass due to increased hepatic lipid oxidation potentially protects from ectopic hepatic lipid accumulation induced by a high fat diet. Indeed, liver lipid content was markedly reduced in mINDY$^{-/-}$ HFD fed mice assessed histologically in liver sections by H&E staining (Figure 4A top), Oil-Red-O staining (Figure 4A middle) and electron microscopy (Figure 4A bottom). Hepatic triglyceride content was reduced by 20% in mINDY$^{-/-}$ mice compared to mINDY$^{+/+}$ mice (Figure 4B). We further analyzed hepatic lipid metabolites using LC/MS-MS (Samuel et al., 2004; Erion et al., 2009). Long chain acyl-CoAs did not differ, but hepatic diacylglycerol (DAG) concentrations were reduced by 40% in mINDY$^{-/-}$ mice (Figure 4D), without a change in hepatic ceramide content (Figure 4D). Hepatic acyl-carnitines tended to be slightly higher in the mINDY$^{-/-}$ mice compared to the mINDY$^{+/+}$ mice (mINDY$^{-/-}$ mice: 671±34 nmol/g liver-tissue vs. mINDY$^{+/+}$: 607±27 nmol/g liver-tissue, P=0.1). Ectopic DAG accumulation has been proposed as a unifying hypothesis for mediating the insulin resistance associated with conditions such as high fat feeding and aging (DAG hypothesis) (Shulman, 2000; Erion and Shulman, 2010; Samuel et al., 2010). Accordingly, DAG accumulation results from the imbalance between supply and utilization of intracellular lipids. Increased DAG content in turn results in activation of novel protein kinase C's (nPKC's) and subsequent impairment in insulin signaling (Shulman, 2000; Samuel et al., 2004; Samuel et al., 2007; Erion and Shulman, 2010; Samuel et al., 2010) In accordance with the DAG hypothesis, mINDY$^{-/-}$ had reduced hepatic membrane PKCε protein content (Figure 4C).

Protection from high fat diet induced insulin resistance

According to the DAG hypothesis, DAG lipid species are major mediators of insulin resistance through activation of nPKCs (Shulman, 2000; Samuel et al., 2004; Samuel et al., 2007; Erion and Shulman, 2010; Samuel et al., 2010). In order to assess the impact of *mIndy* loss on glucose metabolism *in vivo*, intraperitoneal glucose tolerance tests (IPGTT) were performed. Basal plasma glucose and insulin concentrations were decreased in mINDY$^{-/-}$ mice compared to mINDY$^{+/+}$ mice (Supplemental Table S2). The glycemic excursion during the IPGTT was reduced by 20% (area under the curve) and plasma insulin excursion was reduced by 47% (area under the curve) in mINDY$^{-/-}$ mice compared to mINDY$^{+/+}$ mice (Figure 5A and 5B). To discern tissue specific contributions to improved whole body insulin sensitivity, hyperinsulinemic-euglycemic (HE) clamps were performed [Figure 5C and 5D and Supplemental Table S3 (Ayala et al., 2010)]. Consistent with the lower fasting plasma glucose concentrations, basal endogenous glucose production was reduced by 20% in mINDY$^{-/-}$ mice (Figure 5E) and endogenous glucose production during the HE clamp was reduced by 50% in the mINDY$^{-/-}$ mice compared to the mINDY$^{+/+}$ mice (Figure 5E), indicating improved hepatic insulin responsiveness. In addition, peripheral glucose uptake (Figure 5F) by the gastrocnemius muscle (Figure 5G) was increased by 38% in the mINDY$^{-/-}$ mice. This protection from fat-induced muscle insulin resistance in mINDY$^{-/-}$ mice was accompanied by a 35% reduction in skeletal muscle DAG content (Figure 5H).

Reduced transport of citrate into cells could potentially result in lower intracellular citrate concentrations and increased rates of glycolysis (Randle et al., 1963). In order to test this possibility we measured plasma lactate concentrations and rates of whole body glycolysis and non-oxidative glucose metabolism (Supplemental Table S3A-C). Plasma lactate concentrations were found to be lower by 20% in mINDY$^{-/-}$ mice compared to mINDY$^{+/+}$ fed a HFD (data not shown). Rates of glycolysis were similar between mINDY$^{+/+}$, mINDY$^{+/-}$, and mINDY$^{-/-}$ mice, while rates of non-oxidative glucose metabolism tended to be increased in HFD fed mINDY$^{-/-}$ mice and were significantly higher in older mINDY$^{-/-}$ mice (Supplemental Table S3A-C). Taken together these data demonstrate that increases in whole body glycolytic flux are not likely responsible for the increased insulin-stimulated glucose uptake observed in the mINDY$^{-/-}$ mice.

Deletion of *mIndy* increases mitochondrial metabolism via AMPK activation

Citrate infusion studies identified the liver as the main organ of transport action for mINDY. In order to determine the mechanism by which loss of *mIndy* increases whole body energy metabolism, we first performed unbiased microarray analysis on hepatic tissue samples from young mINDY$^{+/+}$ and mINDY$^{-/-}$ mice, without a difference in body composition. Gene set enrichment analysis revealed markedly increased expression of pathways regulating mitochondrial genes, oxidative phosphorylation and electron transport chain genes in the mINDY$^{-/-}$ mice (Figure 6A). Consistent with findings in *D. melanogaster* (Wang et al., 2009), mitochondrial density, assessed by the point counting method using electron microscopy (Bergeron et al. 2001), was increased in mINDY$^{-/-}$ mice (Figure 6B and 6C), as were multiple genes related to the electron transport chain (ETC), TCA-cycle and oxidative phosphorylation (OXPHOS) (Supplemental Table S4). AMP activated protein kinase (AMPK) is a metabolic regulator that is activated by AMP and inhibited by ATP, which promotes mitochondrial biogenesis, insulin sensitivity and fat oxidation (Bergeron et al., 2001). AMPK activity correlates tightly with phosphorylation at Thr172-alpha subunit (phospho-AMPK). Fasted mINDY$^{-/-}$ mice exhibit a 52% reduction in hepatic ATP content (Figure 6D), a 54% reduction in ATP/ADP ratio (Figure 6D) and a 62% increase in Thr172 phosphorylation of the alpha subunit of AMPK (Figure 6E). In line with our observation that skeletal muscle citrate uptake did not differ between mINDY$^{+/+}$ and mINDY$^{-/-}$ mice (Figure 1D), ATP content, AMPK activation, and metabolic gene expression profiles did not differ in skeletal muscle samples (Supplemental Figure S5A and S5B).

Peroxisome proliferator-activated receptor-γ coactivator (PGC)-1α expression, a target of AMPK and a master regulator of mitochondrial biogenesis (Lopez-Lluch et al., 2008), was increased by 64% in liver of the mINDY$^{-/-}$ mice (Figure 6F). Another target of AMPK is acetyl-CoA carboxylase 2 (ACC-2) (Ruderman et al., 1999) ACC-2 serine phosphorylation, which reduces the activity of ACC-2, was also significantly increased in the mINDY$^{-/-}$ mice (Supplemental Figure S5C). Next, we assessed other genes that regulate hepatic lipid oxidation and synthesis and found increased expression in genes that promote fat oxidation in the mINDY$^{-/-}$ mice in liver (Supplemental Figure S5D), but not skeletal muscle (Supplemental Figure S5A and S5B). These data indicate that liver is the main tissue of *mIndy* action. Protein content of hepatic mature sterol regulatory element binding protein (SREBP)-1c, a lipogenic master regulator, was decreased in mINDY$^{-/-}$ mice (Supplemental Figure S5E). This decrease in mature SREBP-1c can also explain the decrease in mitochondrial GPAT (mtGPAT) mRNA expression (Supplemental Figure S5D). In order to assess a causal role of AMPK in mediating changes seen in mINDY$^{-/-}$ mice, lipid synthesis from [^{14}C]-citrate was measured with and without the AMPK inhibitor Compound C in primary hepatocytes. Fatty acid synthesis could not be further increased in mINDY$^{+/+}$ hepatocytes, while AMPK inhibition increased lipid synthesis in the mINDY$^{-/-}$ hepatocytes by 240% (Supplemental Figure S5F). Taken together these data indicate that AMPK

activation is at least in part responsible for the observed increases in hepatic fatty acid oxidation and mitochondrial biogenesis as well as for the decreases in hepatic lipogenesis in the mINDY$^{-/-}$ mice.

Protection from aging induced adiposity and insulin resistance

Reduced expression of *Indy in D. melanogaster* and *C. elegans* increases life span (Rogina et al., 2000; Fei et al., 2004) and reduces specific characteristics of aging in a manner akin to caloric restriction (Wang et al., 2009). Since aging has been shown to be associated with reduced mitochondrial function, ectopic lipid accumulation and muscle insulin resistance (Petersen et al., 2003) we examined how loss of *mIndy* would affect energy and glucose metabolism in older mice. We observed that eight-month old mINDY$^{-/-}$ mice maintained on a regular chow diet had a 17% reduction in body weight, compared to age matched littermate mINDY$^{+/+}$ mice (Figure 7A), together with a reduction in fat mass by 45% (Figure 7B) and an increase in the proportion of lean body mass by 11% (Figure 7C). When comparing three-month old mINDY$^{-/-}$ to eight-month old mINDY$^{-/-}$ mice, proportions of fat mass and lean body mass did not change, while in the eight-month old mINDY$^{+/+}$ mice, fat mass increased (Figure 7B) and lean body mass decreased significantly (Figure 7B). Similar to young mice, energy expenditure was increased in the eight-month old INDY$^{-/-}$ mice compared to eight-month old INDY$^{+/+}$ mice (Supplemental Table S1).

Eight-month old mINDY$^{-/-}$ mice and age-matched mINDY$^{+/+}$ littermates were subjected to hyperinsulinemic-euglycemic clamp studies. Basal glucose and insulin concentrations were reduced by 16% and 29%, respectively, in the older mINDY$^{-/-}$ mice compared to older mINDY$^{+/+}$ mice (Supplemental Table S2). Eight-month old mINDY$^{-/-}$ mice showed preserved insulin sensitivity compared to eight-month old mINDY$^{+/+}$ mice, as reflected by a marked increase in the glucose infusion rate required to maintain euglycemia during the hyperinsulinemic-euglycemic clamp [Figure 7D and Supplemental Table S3 (Ayala et al., 2010)]. Endogenous glucose production (Figure 7E, Supplemental Table S3) during the hyperinsulinemic-euglycemic clamp was two-fold lower in older mINDY$^{-/-}$ mice compared to older mINDY$^{+/+}$ mice reflecting increased hepatic insulin responsiveness in the mINDY$^{-/-}$ mice (Figure 7F). Whole body glucose metabolism during the hyperinsulinemic-euglycemic clamp was increased by 68% in the eight-month old mINDY$^{-/-}$ mice (Figure 7G), which could be attributed to a 27% increase in skeletal muscle glucose transport activity (Figure 7H) and a 43% increase in hepatic non-oxidative glucose metabolism (Supplemental Table S3).

Deletion of *mIndy* mimics various transcriptional aspects of calorie restriction

Decreased *Indy* expression has been proposed to mimic a state of caloric restriction in *D. melanogaster* (Wang et al., 2009; Neretti et al., 2009). We performed unbiased whole-genome microarray based analysis of the transcriptional regulation of pathways in mINDY$^{-/-}$ mice versus mINDY$^{+/+}$ mice and compared them to the regulation of pathways in calorically restricted mice versus *ad libitum* fed mice. Eighty percent of pathways were regulated in a similar fashion in mINDY$^{-/-}$and calorically restricted mice (Supplemental Figure S6A). Furthermore, calorie restriction has been shown to reduce *Indy* mRNA expression in *D. melanogaster*. We investigated whether similar results would be observed after a prolonged fast in mice. Consistent with these results, *mIndy* expression was reduced by 48% in mice starved for 36 hours compared to fed mice (Supplemental Figure S6B). In order to assess the physiological impact of starvation on mINDY$^{-/-}$ mice, we compared mINDY$^{+/+}$ and mINDY$^{-/-}$ animals that were fasted for 24h and 48h hours. mINDY$^{-/-}$ mice showed greater weight loss and markedly reduced glycogen stores after 24h (Supplemental Figure S7A and 7B), while plasma glucose and insulin concentrations tended to be lower after 24h (Supplemental Figure S7C and S7D).

DISCUSSION

Reduced expression of *Indy* and its homologues increases life span in *D. melanogaster* and *C. elegans* (Rogina et al., 2000; Fei et al., 2004). These findings have been compared to caloric restriction (Wang et al., 2009), an intervention that extends lifespan in divers species including mammals (Colman et al., 2009; Fontana and Klein, 2007). Here, we show that deletion of the mammalian *Indy* homologue in mice reduces adiposity, prevents lipid accumulation into liver and skeletal muscle and increases insulin sensitivity under HFD conditions and during aging. Loss of *mIndy* augments energy expenditure associated with increased hepatic fat oxidation and attenuates hepatic lipogenesis. Strikingly, caloric intake is not decreased in mINDY$^{-/-}$ mice.

Consistent with previous studies (Knauf et al., 2002; Knauf et al., 2006) we show that mINDY is a high capacity plasma membrane transporter for citrate (K_m 49±9 μM). Cytosolic citrate either originates from mitochondria, where it is generated in one turn of the citric acid cycle for the ultimate conversion into ATP, or citrate it is taken up across the plasma membrane from the blood stream, in which it circulates in relatively high concentrations (~50-150 μM) (Palmieri, 2004). Citrate is cleaved to oxaloacetate and acetyl-CoA, which provides the immediate carbon source for the biosynthesis of fatty acids, triacylglycerols and cholesterol (Muoio and Newgard, 2008). Fatty acids provide >70% of the energy requirements of the liver (Alves et al., 2011). We show that loss of *mIndy* reduces hepatocellular fatty acid- and sterol-generation and promotes hepatic lipid oxidation, and thus, reduces ectopic storage of fat in the liver. In line with this, enhancing the function of the human *mIndy* gene product dose-dependently increases the cellular uptake of [^{14}C]-citrate as well as its incorporation into intracellular lipids (Inoue et al., 2003).

Deletion of *mIndy* induces a state of hepatic energy depletion as reflected by the decrease in hepatic ATP content and ATP/ADP ratio. Increased AMP and decreased ATP concentrations are major activators of AMPK (Zhang et al., 2009). Our data suggests that reduced uptake of mINDY-substrates leads to depletion of biochemical energy, which results in the activation of AMPK. Recent studies have shown that intracerebroventricular injection of citrate inhibits hypothalamic AMPK, which is consistent with this possibility (Stoppa et al., 2008). AMPK induces hepatic fatty acid oxidation through phosphorylation and inhibition of ACC-2 activity, reduces lipid generation by inhibition of SREBP-1c (Kahn et al., 2005) and promotes the generation of ATP by inducing mitochondrial biogenesis through activation of PGC-1α (Bergeron et al., 2001; Zhang et al., 2009). The *mIndy* deleted phenotype is consistent with these traits.

Under certain conditions, cytosolic tri- or dicarboxylates are exchanged for mitochondrial citrate, which in turn lacks for ATP generation (Muoio and Newgard, 2008). Moreover, cytosolic citrate acts as a turnstile in fuel sensing and signaling, by allosteric activation of ACC-2 (Saha et al., 1999; Ruderman et al., 1999) and it might inhibit glycolysis in the presence of ATP (Bosca et al., 1985). Together, these data indicate that citrate also acts as a signaling molecule and consequently, reduced citrate signaling activity might contribute to the *mIndy*-deleted phenotype. Yet, our data does not completely rule out the possibility that mINDY also exerts effects independent of the uptake mechanism.

mIndy expression and activity is most abundant in liver and much lower in other organs and tissues, but loss of *mIndy* not only affected hepatic metabolism but also increased energy expenditure, which in turn reduced whole body fat content, as well as skeletal muscle lipid storage and it increased insulin-stimulated glucose uptake into skeletal muscle. These results show similarities to liver-specific overexpression of AMPK (Yang et al., 2008) in HFD fed mice and other mouse models with specifically targeted tissues and organs (Oyadomari et

al., 2008; Ahmadian et al., 2009; Dean et al., 2009). It is likely that the relatively minor phenotype observed in the young mINDY$^{-/-}$ mice can also be attributed to the compensatory increase in expression of *SLC13A3 (*NaDC3*)*. With high fat feeding, the compensatory increase in *SLC13A3* is abolished, and the metabolic phenotype is fully developed.

Energy expenditure increases in response to water ingestion through sympathetic nervous system activation (Boschmann et al., 2007; Lechner et al., 2011). It is therefore possible that augmented water drinking, as observed in the HFD-fed and older mINDY$^{-/-}$ mice, could have contributed to the observed increase in energy expenditure. However, this event would not explain the increase in energy expenditure in the young, regular chow fed mINDY$^{-/-}$ mice that have a normal drinking pattern.

Caloric restriction promotes mitochondrial biogenesis and function (Hunt et al., 2006; Lopez-Lluch et al., 2008). Caloric restriction is effective in correcting the unfavorable metabolic consequences of high fat feeding and aging (Fontana and Klein, 2007). We show that in calorically restricted mice, as compared to isocalorically fed mice, 80% of transcriptionally regulated pathways change in the same direction as in the mINDY$^{-/-}$ mice. Functionally, loss of *mIndy* also mimics many aspects of calorically restriction. Moreover, in flies and nematodes, both, reduced expression of *Indy*, as well as caloric restriction, prolong life span (Rogina et al., 2000; Fei et al., 2004) and AMPK has been shown to be the mediator of longevity in response to most dietary restriction regimens in *C.elegans* (Schulz et al., 2007; Greer and Brunet, 2009; Mair et al., 2011). In addition, caloric restriction does not increase life span further in flies with reduced *Indy* expression (Toivonen et al., 2007; Wang et al., 2009), pointing to similar underlying mechanisms in both conditions. These data suggest that *mIndy* may be a key mediator of the beneficial effects of dietary energy restriction. Since prolonged caloric restriction is very difficult to achieve in humans, our observations raise the tantalizing possibility that modulating the levels or function of *mIndy* could lead to some of the health promoting effects of calorie restriction, without requiring severe caloric restriction.

Hepatic lipid content is strongly associated with hepatic insulin resistance (Samuel et al., 2010). A unifying hypothesis is that insulin resistance in liver and skeletal muscle develops when there is an imbalance between supply and utilization of intracellular lipid leading to net accumulation of intracellular diacylglycerol (DAG hypothesis) (Shulman, 2000; Erion and Shulman, 2010). In contrast, with aging, declines in mitochondrial function may contribute to net accumulation of intracellular DAGs (Petersen et al., 2003; Reznick et al., 2007; Lee et al., 2010). Consistent with this hypothesis, loss of *mIndy* reduces hepatic DAG concentrations, decreases membrane PKCε content, and protects from hepatic insulin resistance associated with high fat feeding and aging.

In summary, we show that the deletion of the mammalian homologue of Drosophila *Indy*, protects mice from HFD-induced and age-associated insulin resistance, which is at least in part mediated by activation of AMPK with subsequent induction of mitochondrial biogenesis via PGC-1α, increased hepatic lipid oxidation and energy expenditure, as well as reduced hepatic lipid generation. Our data suggest that *mIndy* may be an attractive therapeutic target for the treatment of non-alcoholic fatty liver disease, obesity and type 2 diabetes.

EXPERIMENTAL PROCEDURES

Generation of mice

A detailed description is given in the Supplemental Methods Section

Cloning of mouse mINDY and uptake assays

Uptake assays were performed as described (Seithel et al., 2007). Shortly, the cDNA encoding mouse mINDY was cloned using a PCR-based approach. HEK293 cells were transfected with pIndy-mouse.31 using Effectene transfection reagent (Qiagen, Hilden, Germany). Uptake assays were performed using HEK-mIndy cells and HEK-Co/418 cells transfected with the empty expression vector pcDNA3.1(+) serving as control cells. [1,5-^{14}C]citric acid and [1,4-^{14}C]succinate (Hartmann Analytic, Germany) were dissolved in uptake buffer and unlabeled citric acid or succinate was added to the final concentration mentioned. The cells were incubated with the uptake solution for 10 min as described (Seithel et al., 2007). The intracellular accumulation of radioactivity was detected by liquid scintillation counting (Perkin Elmer Life Sciences). mINDY-mediated citric acid or succinate net uptake was obtained by subtracting the uptake in vector-transfected HEK-Co/418 cells from that in mINDY-expressing HEK cells. K_m values were determined by fitting the data to a non-linear regression curve fit [Michaelis-Menten-fit (Prism 5, GraphPad Software, San Diego, CA)].

Basal Study

Mice were housed under controlled temperature (22 ± 2°C) and lighting (12 hrs of light, 0700–1900 hours; 12 hrs of dark, 1900–0700 hours) with free access to water and food. mINDY$^{+/+}$, mINDY$^{+/-}$, and mINDY$^{-/-}$ were fed a regular chow diet (TD2018; Harlan Teklad, Madison, WI). Dough high fat diet (HFD, 55% fat by calories; TD 93075; Harlan Teklad) was fed at the age of 5-6 weeks for a period of 6-8 weeks in order to assess the effect of HFD on metabolic regulation. Fat and lean body masses were assessed by ^{1}H-magnetic resonance spectroscopy (Bruker BioSpin, Billerica, MA). Comprehensive animal metabolic monitoring system (CLAMS; Columbus Instruments, Columbus, OH) was used to evaluate activity, food consumption, and energy expenditure. Drinking was assessed by a computed system counting consumed water droplets. More details are given in the Supplemental Methods Section.

Hyperinsulinemic-euglycemic clamp studies and [^{14}C] citrate infusion studies

Hyperinsulinemic euglycemic clamp studies were conducted as described (Jurczak et al., 2011; Pajvani et al, 2011). Details are given in the Supplemental Methods Section.

Biochemical analysis and calculations

Calculations were done as described (Chutkow et al., 2010; Jornayvaz et al., 2011) and details are given in the Supplemental Methods Section.

mRNA quantification by real-time PCR

Liver total RNA was isolated using the RNeasy kit per manufacturer's instructions (Invitrogen Corporation, CA, USA) and qPCR was performed as described (Lee et al., 2010). Primer sequences are displayed in Supplemental Table S5.

Immunoblots

Immunoblots were performed as described (Zhang et al., 2010). Phospho-AMPK and AMPK (Cell Signaling Technology, MA, USA), phospho-ACC2 and ACC2 (Santa Cruz Biotechnology Inc., CA, USA), PGC-1α (Cell Signaling Technology, MA, USA), SREBP-1c (Santa Cruz Biotechnology Inc., CA, USA), β-actin (Abcam, MA, USA) or Gapdh (Cell Signaling Technology, MA, USA) were used as primary antibodies. PKCε assays were performed as described (Samuel et al., 2004).

Transmission Electron Microscopy Analysis

Individual liver samples were prepared as described (Bergeron et al., 2001). Only cross-sections of liver were examined for quantification of mitochondrial density. For each individual liver slice, six random pictures were taken at a magnification of 7,100× and printed at a final magnification of 18,250×. The volume density of mitochondria was estimated using the point-counting method (Bergeron et al., 2001) by a sample blinded EM-technician. The average volume density was calculated for each individual mouse liver and was used to calculate the average volume density for each genotype.

Lipid oxidation and lipid synthesis in primary hepatocytes

Details are given in the Supplemental Methods Section. Shortly, primary hepatocytes were isolated at the Yale Liver Center. 10^6 cells per flask were incubated in Williams E Medium with 0.1 mM [1-^{14}C]oleate (Amersham Biosciences, NJ, USA). After 1h, incubations were quenched with 20% perchloric acid and hyamine hydroxide was added to the filter paper in the center well to collect [$^{14}CO^2$]. After 1h on ice, filter paper and perchloric acid–soluble ^{14}C-radioactivity was counted in a scintillation counter (New et al., 1999). Reactions were normalized to protein amounts. Lipid synthesis was assessed in cultures of isolated hepatocytes (10^6) with William E medium, 10 nM insulin and 10 μM [1,5-^{14}C]-citric acid (Movarek Biochemicals, CA, USA) for 24h. Cells were homogenized in PBS and mixed with 10N NaOH and ethanol. Sterols were extracted with hexanes twice. The lower layer, containing sterols, were first mixed with 10M H_2SO_4 and then extracted with hexanes. The upper layer was then dried and counted in a scintillation counter to determine [^{14}C]-fatty acids.

Oxygen consumption in liver homogenate

Oxygen consumption was assessed with a Clark-type oxygen electrode (Hansatech Instruments, UK) as described (Lee et al., 2010) with the exception that liver homogenate was used.

Plasma metabolite extraction, measurements, alignment and normalization

30μl of the murine plasma was extracted with 400μl 100% Methanol at −20°C (^{13}C-sorbitol was added as an internal standard). After centrifugation the supernatant was vacuum dried. GC-TOF-MS metabolite profiling was performed on a Leco Pegasus 3 time-of-flight mass spectrometer (Leco, St.Joseph, MI, USA). The Direct Thermal Desorption injector (ATAS GL International, The Netherlands) was coupled to an HP 5890 gas chromatograph and an autosampler with automatic derivatisation and linear exchange. This eliminates the impact of potential degradation or synthesis artifacts and sample carryover. During the derivatisation there was also added a retention time index standard mixture. For detailed information refer to (Lisec et al., 2006; Catchpole et al., 2009). Chromatogram acquisition parameters were those described previously (Weckwerth et al., 2004). The results were exported from Leco Chroma TOF software (version 3.25) as cdf-files. Peak detection, retention time alignment, and library matching were performed with the R-script “Target Search” (Cuadros-Inostroza et al., 2009). Relative peak intensities were normalized by the median of ^{13}C-sorbitol intensities of all samples by the ^{13}C-sorbitol intensity of the respective sample and $\log_{10}$ transformed.

ATP and ADP content

Liver extracts were prepared for high field NMR analysis by homogenizing 100mg of tissue in 0.9% perchloric acid (2 v/w) and ethanol (2v/w). After homogenization, samples were centrifuged and the supernatant was extracted and neutralized with K_2CO_3, lyophilized and resuspended in buffer containing 20mM HEPES (pH 6), 20mM EDTA, 0.5M KCl, 50%

D_2O and 1mM of phenylphosphonic acid (Sigma-Aldrich, St Louis, MO). ATP and ADP content was analyzed using a Bruker 5-mm ^{31}P-NMR probe in an 11.7-T vertical magnet. Spectra were acquired with TR = 1 s, NS = 2048, and 32K data.

Microarray analysis

Microarray data was analyzed using DIANE 6.0,a spreadsheet-based microarray analysis program based on SAS JMP7.0 system. All Raw data is available in GEO database. Details are given in the Supplemental Methods Section.

Statistical Analysis

A two-tailed Student's t-test was used to test differences between mINDY$^{+/+}$ and mINDY$^{-/-}$ mice. One-way ANOVA analysis was performed for multiple comparisons, two-way ANOVA was performed to test multiple time dependent effects. Values are presented as mean±SEM; $P<0.05$ was considered statistically significant.

Supplementary Material

Refer to Web version on PubMed Central for supplementary material.

Acknowledgments

We thank Xiaoxian Ma, Mario Kahn, Blas Guigni, Yanna Kosover, and Debbie C. Jiang for their excellent technical support in these studies, the UCHC transgenic facility for making the mice, and Lothar Willmitzer, Max-Planck Institute of Plant Physiology Potsdam, for help with plasma metabolite measurements. This work was in part supported by the United States Public Health Service grants: R01 DK-40936 (GIS), U24 DK-59635 (VS, GS), P30 DK-45735, P30 DK-034989, R37 AG-16667 (SLH) and the intramural research program of the National Institute of Aging and a Mentor-Based Postdoctoral Fellowship Award from the American Diabetes Association (GIS). ALB was supported by DFG grant Bi1292/2-1 from the German Research Association (Deutsche Forschungsgemeinschaft) and a project grant from the German Diabetes Association (Deutsche Diabetes Gesellschaft).

Reference List

Ahmadian M, Duncan RE, Varady KA, Frasson D, Hellerstein MK, Birkenfeld AL, Samuel VT, Shulman GI, Wang Y, Kang C, Sul HS. Adipose overexpression of desnutrin promotes fatty acid use and attenuates diet-induced obesity. Diabetes. 2009; 58:855–866. [PubMed: 19136649]

Alves TC, Befroy DE, Kibbey RG, Kahn M, Codella R, Carvalho RA, Petersen KF, Shulman GI. Regulation of hepatic fat and glucose oxidation in rats with lipid-induced hepatic insulin resistance. Hepatology. 2011 epub.

Ayala JE, Samuel VT, Morton GJ, Obici S, Croniger CM, Shulman GI, Wasserman DH, McGuinness OP. Standard operating procedures for describing and performing metabolic tests of glucose homeostasis in mice. Dis. Model. Mech. 2010; 3:525–534. [PubMed: 20713647]

Bergeron R, Ren JM, Cadman KS, Moore IK, Perret P, Pypaert M, Young LH, Semenkovich CF, Shulman GI. Chronic activation of AMP kinase results in NRF-1 activation and mitochondrial biogenesis. Am. J. Physiol Endocrinol. Metab. 2001; 281:E1340–E1346. [PubMed: 11701451]

Bosca L, Aragon JJ, Sols A. Modulation of muscle phosphofructokinase at physiological concentration of enzyme. J. Biol. Chem. 1985; 260:2100–2107. [PubMed: 2982809]

Boschmann M, Steiniger J, Franke G, Birkenfeld AL, Luft FC, Jordan J. Water drinking induces thermogenesis through osmosensitive mechanisms. J. Clin. Endocrinol. Metab. 2007; 92:3334–3337. [PubMed: 17519319]

Catchpole G, Platzer A, Weikert C, Kempkensteffen C, Johannsen M, Krause H, Jung K, Miller K, Willmitzer L, Selbig J, Weikert S. Metabolic profiling reveals key metabolic features of renal cell carcinoma. J. Cell Mol. Med. 2009

Chutkow WA, Birkenfeld AL, Brown JD, Lee HY, Frederick DW, Yoshioka J, Patwari P, Kursawe R, Cushman SW, Plutzky J, Shulman GI, Samuel VT, Lee RT. Deletion of the {alpha}-arrestin protein

Txnip in mice promotes adiposity and adipogenesis while preserving insulin sensitivity. Diabetes. 2010

Colman RJ, Anderson RM, Johnson SC, Kastman EK, Kosmatka KJ, Beasley TM, Allison DB, Cruzen C, Simmons HA, Kemnitz JW, Weindruch R. Caloric restriction delays disease onset and mortality in rhesus monkeys. Science. 2009; 325:201–204. [PubMed: 19590001]

Cuadros-Inostroza A, Caldana C, Redestig H, Kusano M, Lisec J, Pena-Cortes H, Willmitzer L, Hannah MA. TargetSearch--a Bioconductor package for the efficient preprocessing of GC-MS metabolite profiling data. BMC. Bioinformatics. 2009; 10:428. [PubMed: 20015393]

Dean JT, Tran L, Beaven S, Tontonoz P, Reue K, Dipple KM, Liao JC. Resistance to diet-induced obesity in mice with synthetic glyoxylate shunt. Cell Metab. 2009; 9:525–536. [PubMed: 19490907]

Erion DM, Ignatova ID, Yonemitsu S, Nagai Y, Chatterjee P, Weismann D, Hsiao JJ, Zhang D, Iwasaki T, Stark R, Flannery C, Kahn M, Carmean CM, Yu XX, Murray SF, Bhanot S, Monia BP, Cline GW, Samuel VT, Shulman GI. Prevention of hepatic steatosis and hepatic insulin resistance by knockdown of cAMP response element-binding protein. Cell Metab. 2009; 10:499–506. [PubMed: 19945407]

Erion DM, Shulman GI. Diacylglycerol-mediated insulin resistance. Nat. Med. 2010; 16:400–402. [PubMed: 20376053]

Fei YJ, Inoue K, Ganapathy V. Structural and functional characteristics of two sodium-coupled dicarboxylate transporters (ceNaDC1 and ceNaDC2) from Caenorhabditis elegans and their relevance to life span. J. Biol. Chem. 2003; 278:6136–6144. [PubMed: 12480943]

Fei YJ, Liu JC, Inoue K, Zhuang L, Miyake K, Miyauchi S, Ganapathy V. Relevance of NAC-2, an Na +-coupled citrate transporter, to life span, body size and fat content in Caenorhabditis elegans. Biochem. J. 2004; 379:191–198. [PubMed: 14678010]

Fontana L, Klein S. Aging, adiposity, and calorie restriction. JAMA. 2007; 297:986–994. [PubMed: 17341713]

Gopal E, Miyauchi S, Martin PM, Ananth S, Srinivas SR, Smith SB, Prasad PD, Ganapathy V. Expression and functional features of NaCT, a sodium-coupled citrate transporter, in human and rat livers and cell lines. Am. J. Physiol Gastrointest. Liver Physiol. 2007; 292:G402–G408. [PubMed: 16973915]

Greer EL, Brunet A. Different dietary restriction regimens extend lifespan by both independent and overlapping genetic pathways in C. elegans. Aging Cell. 2009; 8:113–127. [PubMed: 19239417]

Hunt ND, Hyun DH, Allard JS, Minor RK, Mattson MP, Ingram DK, de Cabo R. Bioenergetics of aging and calorie restriction. Ageing Res. Rev. 2006; 5:125–143. [PubMed: 16644290]

Hursting SD, Lavigne JA, Berrigan D, Perkins SN, Barrett JC. Calorie restriction, aging, and cancer prevention: mechanisms of action and applicability to humans. Annu. Rev. Med. 2003; 54:131–152. [PubMed: 12525670]

Inoue K, Fei YJ, Huang W, Zhuang L, Chen Z, Ganapathy V. Functional identity of Drosophila melanogaster Indy as a cation-independent, electroneutral transporter for tricarboxylic acid-cycle intermediates. Biochem. J. 2002a; 367:313–319. [PubMed: 12186628]

Inoue K, Zhuang L, Maddox DM, Smith SB, Ganapathy V. Structure, function, and expression pattern of a novel sodium-coupled citrate transporter (NaCT) cloned from mammalian brain. J. Biol. Chem. 2002b; 277:39469–39476. [PubMed: 12177002]

Inoue K, Zhuang L, Maddox DM, Smith SB, Ganapathy V. Human sodium-coupled citrate transporter, the orthologue of Drosophila Indy, as a novel target for lithium action. Biochem. J. 2003; 374:21–26. [PubMed: 12826022]

Jornayvaz FR, Birkenfeld AL, Jurczak MJ, Kanda S, Guigni BA, Jiang DC, Zhang D, Lee HY, Samuel VT, Shulman GI. Hepatic insulin resistance in mice with hepatic overexpression of diacylglycerol acyltransferase 2. Proc. Natl. Acad. Sci. U. S. A. 2011 epub.

Jurczak MJ, Lee HY, Birkenfeld AL, Jornayvaz FR, Frederick DW, Pongratz RL, Zhao X, Moeckel GW, Samuel VT, Whaley JM, Shulman GI, Kibbey RG. SGLT2 Deletion Improves Glucose Homeostasis and Preserves Pancreatic {beta}-Cell Function. Diabetes. 2011; 60:890–898. [PubMed: 21357472]

Kahn BB, Alquier T, Carling D, Hardie DG. AMP-activated protein kinase: ancient energy gauge provides clues to modern understanding of metabolism. Cell Metab. 2005; 1:15–25. [PubMed: 16054041]

Knauf F, Mohebbi N, Teichert C, Herold D, Rogina B, Helfand S, Gollasch M, Luft FC, Aronson PS. The life-extending gene Indy encodes an exchanger for Krebs-cycle intermediates. Biochem. J. 2006; 397:25–29. [PubMed: 16608441]

Knauf F, Rogina B, Jiang Z, Aronson PS, Helfand SL. Functional characterization and immunolocalization of the transporter encoded by the life-extending gene Indy. Proc. Natl. Acad. Sci. U. S. A. 2002; 99:14315–14319. [PubMed: 12391301]

Lechner SG, Markworth S, Poole K, Smith ES, Lapatsina L, Frahm S, May M, Pischke S, Suzuki M, Ibanez-Tallon I, Luft FC, Jordan J, Lewin GR. The molecular and cellular identity of peripheral osmoreceptors. Neuron. 2011; 69:332–344. [PubMed: 21262470]

Lee HY, Choi CS, Birkenfeld AL, Alves TC, Jornayvaz FR, Jurczak MJ, Zhang D, Woo DK, Shadel GS, Ladiges W, Rabinovitch PS, Santos JH, Petersen KF, Samuel VT, Shulman GI. Targeted expression of catalase to mitochondria prevents age-associated reductions in mitochondrial function and insulin resistance. Cell Metab. 2010; 12:668–674. [PubMed: 21109199]

Lisec J, Schauer N, Kopka J, Willmitzer L, Fernie AR. Gas chromatography mass spectrometry-based metabolite profiling in plants. Nat. Protoc. 2006; 1:387–396. [PubMed: 17406261]

Lopez-Lluch G, Hunt N, Jones B, Zhu M, Jamieson H, Hilmer S, Cascajo MV, Allard J, Ingram DK, Navas P, de Cabo R. Calorie restriction induces mitochondrial biogenesis and bioenergetic efficiency. Proc. Natl. Acad. Sci. U. S. A. 2006; 103:1768–1773. [PubMed: 16446459]

Lopez-Lluch G, Irusta PM, Navas P, de Cabo R. Mitochondrial biogenesis and healthy aging. Exp. Gerontol. 2008; 43:813–819. [PubMed: 18662766]

Mair W, Morantte I, Rodrigues AP, Manning G, Montminy M, Shaw RJ, Dillin A. Lifespan extension induced by AMPK and calcineurin is mediated by CRTC-1 and CREB. Nature. 2011; 470:404–408. [PubMed: 21331044]

Muoio DM, Newgard CB. Mechanisms of disease: molecular and metabolic mechanisms of insulin resistance and beta-cell failure in type 2 diabetes. Nat. Rev. Mol. Cell Biol. 2008; 9:193–205. [PubMed: 18200017]

Neretti N, Wang PY, Brodsky AS, Nyguyen HH, White KP, Rogina B, Helfand SL. Long-lived Indy induces reduced mitochondrial reactive oxygen species production and oxidative damage. Proc. Natl. Acad. Sci. U. S. A. 2009; 106:2277–2282. [PubMed: 19164521]

Neschen S, Morino K, Hammond LE, Zhang D, Liu ZX, Romanelli AJ, Cline GW, Pongratz RL, Zhang XM, Choi CS, Coleman RA, Shulman GI. Prevention of hepatic steatosis and hepatic insulin resistance in mitochondrial acyl-CoA:glycerol-sn-3-phosphate acyltransferase 1 knockout mice. Cell Metab. 2005; 2:55–65. [PubMed: 16054099]

New KJ, Krauss S, Elliott KR, Quant PA. Comparisons of flux control exerted by mitochondrial outer-membrane carnitine palmitoyltransferase over ketogenesis in hepatocytes and mitochondria isolated from suckling or adult rats. Eur. J. Biochem. 1999; 259:684–691. [PubMed: 10092853]

Nishimura M, Naito S. Tissue-specific mRNA expression profiles of human solute carrier transporter superfamilies. Drug Metab Pharmacokinet. 2008; 23:22–44. [PubMed: 18305372]

Oyadomari S, Harding HP, Zhang Y, Oyadomari M, Ron D. Dephosphorylation of translation initiation factor 2alpha enhances glucose tolerance and attenuates hepatosteatosis in mice. Cell Metab. 2008; 7:520–532. [PubMed: 18522833]

Pajvani UB, Shawber CJ, Birkenfeld AL, Samuel VT, Shulman GI, Kitajewski J, Accili D. Inhibition of Notch Signaling Ameliorates Obesity Induced Insulin Resistance Through FoxO1 Dependent and Independent Mechanisms. Nat. Med. 2011 In Press.

Palmieri F. The mitochondrial transporter family (SLC25): physiological and pathological implications. Pflugers Arch. 2004; 447:689–709. [PubMed: 14598172]

Petersen KF, Befroy D, Dufour S, Dziura J, Ariyan C, Rothman DL, DiPietro L, Cline GW, Shulman GI. Mitochondrial dysfunction in the elderly: possible role in insulin resistance. Science. 2003; 300:1140–1142. [PubMed: 12750520]

Randle PJ, Garland PB, Hales CN, Newsholme EA. The glucose fatty-acid cycle. Its role in insulin sensitivity and the metabolic disturbances of diabetes mellitus. Lancet. 1963; 1:785–789. [PubMed: 13990765]

Reznick RM, Zong H, Li J, Morino K, Moore IK, Yu HJ, Liu ZX, Dong J, Mustard KJ, Hawley SA, Befroy D, Pypaert M, Hardie DG, Young LH, Shulman GI. Aging-associated reductions in AMP-activated protein kinase activity and mitochondrial biogenesis. Cell Metab. 2007; 5:151–156. [PubMed: 17276357]

Rinaldo P, Matern D, Bennett MJ. Fatty acid oxidation disorders. Annu. Rev. Physiol. 2002; 64:477–502. [PubMed: 11826276]

Rogina B, Reenan RA, Nilsen SP, Helfand SL. Extended life-span conferred by cotransporter gene mutations in Drosophila. Science. 2000; 290:2137–2140. [PubMed: 11118146]

Ruderman NB, Saha AK, Vavvas D, Witters LA. Malonyl-CoA, fuel sensing, and insulin resistance. Am. J. Physiol. 1999; 276:E1–E18. [PubMed: 9886945]

Saha AK, Laybutt DR, Dean D, Vavvas D, Sebokova E, Ellis B, Klimes I, Kraegen EW, Shafrir E, Ruderman NB. Cytosolic citrate and malonyl-CoA regulation in rat muscle in vivo. Am. J. Physiol. 1999; 276:E1030–E1037. [PubMed: 10362615]

Samuel VT, Liu ZX, Qu X, Elder BD, Bilz S, Befroy D, Romanelli AJ, Shulman GI. Mechanism of hepatic insulin resistance in non-alcoholic fatty liver disease. J. Biol. Chem. 2004; 279:32345–32353. [PubMed: 15166226]

Samuel VT, Liu ZX, Wang A, Beddow SA, Geisler JG, Kahn M, Zhang XM, Monia BP, Bhanot S, Shulman GI. Inhibition of protein kinase Cepsilon prevents hepatic insulin resistance in nonalcoholic fatty liver disease. J. Clin. Invest. 2007; 117:739–745. [PubMed: 17318260]

Samuel VT, Petersen KF, Shulman GI. Lipid-induced insulin resistance: unravelling the mechanism. Lancet. 2010; 375:2267–2277. [PubMed: 20609972]

Schulz TJ, Zarse K, Voigt A, Urban N, Birringer M, Ristow M. Glucose restriction extends Caenorhabditis elegans life span by inducing mitochondrial respiration and increasing oxidative stress. Cell Metab. 2007; 6:280–293. [PubMed: 17908557]

Seithel A, Eberl S, Singer K, Auge D, Heinkele G, Wolf NB, Dorje F, Fromm MF, Konig J. The influence of macrolide antibiotics on the uptake of organic anions and drugs mediated by OATP1B1 and OATP1B3. Drug Metab Dispos. 2007; 35:779–786. [PubMed: 17296622]

Shulman GI. Cellular mechanisms of insulin resistance. J. Clin. Invest. 2000; 106:171–176. [PubMed: 10903330]

Stoppa GR, Cesquini M, Roman EA, Prada PO, Torsoni AS, Romanatto T, Saad MJ, Velloso LA, Torsoni MA. Intracerebroventricular injection of citrate inhibits hypothalamic AMPK and modulates feeding behavior and peripheral insulin signaling. J. Endocrinol. 2008; 198:157–168. [PubMed: 18469022]

Toivonen JM, Walker GA, Martinez-Diaz P, Bjedov I, Driege Y, Jacobs HT, Gems D, Partridge L. No influence of Indy on lifespan in Drosophila after correction for genetic and cytoplasmic background effects. PLoS. Genet. 2007; 3:e95. [PubMed: 17571923]

Wang PY, Neretti N, Whitaker R, Hosier S, Chang C, Lu D, Rogina B, Helfand SL. Long-lived Indy and calorie restriction interact to extend life span. Proc. Natl. Acad. Sci. U. S. A. 2009; 106:9262–9267. [PubMed: 19470468]

Weckwerth W, Wenzel K, Fiehn O. Process for the integrated extraction, identification and quantification of metabolites, proteins and RNA to reveal their co-regulation in biochemical networks. Proteomics. 2004; 4:78–83. [PubMed: 14730673]

Wellen KE, Hatzivassiliou G, Sachdeva UM, Bui TV, Cross JR, Thompson CB. ATP-citrate lyase links cellular metabolism to histone acetylation. Science. 2009; 324:1076–1080. [PubMed: 19461003]

Yang J, Maika S, Craddock L, King JA, Liu ZM. Chronic activation of AMP-activated protein kinase-alpha1 in liver leads to decreased adiposity in mice. Biochem. Biophys. Res. Commun. 2008; 370:248–253. [PubMed: 18381066]

Zhang BB, Zhou G, Li C. AMPK: an emerging drug target for diabetes and the metabolic syndrome. Cell Metab. 2009; 9:407–416. [PubMed: 19416711]

Zhang D, Christianson J, Liu ZX, Tian L, Choi CS, Neschen S, Dong J, Wood PA, Shulman GI. Resistance to high-fat diet-induced obesity and insulin resistance in mice with very long-chain acyl-CoA dehydrogenase deficiency. Cell Metab. 2010; 11:402–411. [PubMed: 20444420]

Highlights

- An *mIndy (SLC13A5)* knockout mouse was generated.
- Loss of *mIndy* decreases hepatic ATP/ADP ratio and activates AMPK.
- *mIndy* deletion promotes mitochondrial biogenesis and energy expenditure.
- Loss of *mIndy* protects from diet- and age-associated insulin resistance.

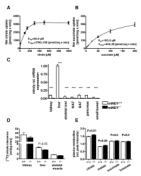

Figure 1.

mIndy tissue distribution and functional characteristics. A and B) mINDY transport kinetics for citrate (A) and succinate (B). HEK293 cells were transfected with the plasmids pIndy-mouse.3.1 or empty expression vector pcDNA3.1(+). Uptake assays were performed in HEK-mIndy cells and HEK-Co/418 cells transfected with the empty expression vector pcDNA3.1(+) serving as control cells. Net-uptake is expressed as the difference between the uptake of substrates into HEK-mIndy cells and HEK-Co/418 cells (n=3-6 for each concentration). K_m values were determined by fitting the data to a non-linear regression curve fit. C) *mIndy* mRNA tissue expression in $mINDY^{+/+}$ and $mINDY^{-/-}$ mice (n=3-4). D) [^{14}C]-citrate clearance in $mINDY^{+/+}$ and $mINDY^{-/-}$ mice *in vivo* (n=6). E) Relative mINDY-substrate plasma concentrations. Plasma citrate concentration is increased in the $mINDY^{-/-}$ mice, in which the cellular uptake of citrate is reduced (n=7-8),***P<0.01, all error bars represent SEM, see also Figures S1 and S2

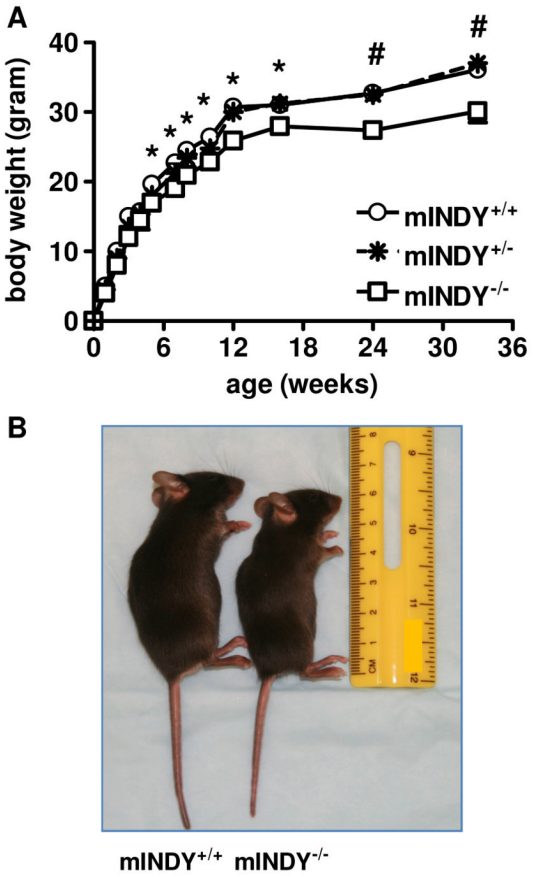

Figure 2.

mINDY mice characteristics. A) Time course of body weight over a nine months period (n=9-15). Differences in body weight increase with time. B) Representative photographs of mINDY$^{+/+}$ and mINDY$^{-/-}$ mice. Body lengths of mINDY$^{+/+}$ and mINDY$^{-/-}$ mice are given in Supplemental Figure S3. *P<0.05, #P<0.01, all error bars represent SEM, see also Figure S3.

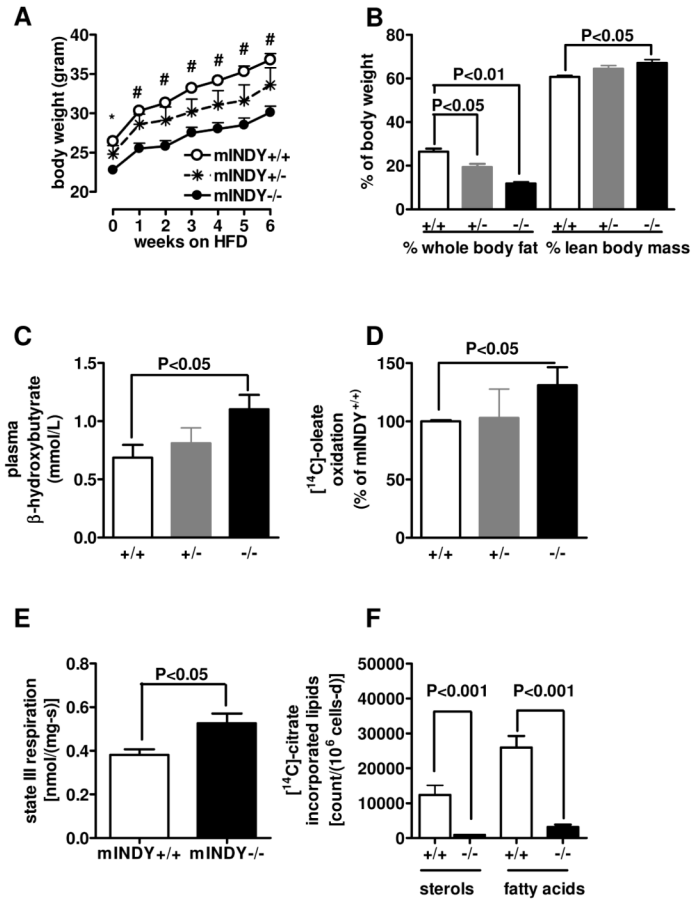

Figure 3.

mINDY mice are protected from HFD induced obesity. A) Body weight of mINDY$^{+/+}$, mINDY$^{+/-}$and mINDY$^{-/-}$ mice on a 6 week HFD (n=8). B) Whole body fat content and lean body mass after a 6 week HFD in the indicated phenotype, as assessed by ^{1}H magnetic resonance spectroscopy (n=8). Body fat is reduced in HFD fed mINDY$^{-/-}$ mice. C) Plasma β-hydroxybutyrate, a marker of hepatic lipid oxidation, is increased in HFD fed mINDY$^{-/-}$ mice (n=7) D) Lipid oxidation from [1-^{14}C]oleate is increased in primary hepatocytes mINDY$^{-/-}$ mice (n=5). E) State III oxygen consumption in liver homogenate from mINDY$^{-/-}$ mice is increased (n=3). F) Lipid synthesis from [^{14}C]citrate is reduced by ~ 90% in mINDY$^{-/-}$ primary hepatocytes (n=6). *P<0.05, #P<0.01, all error bars represent SEM, see also Figure S4

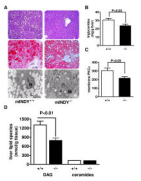

Figure 4.

Protection from HFD induced hepatic steatosis. A) Representative H&E stains (top), Oil-Red-O stains (middle) and electron microscopic magnifications of liver samples from 6 week HFD fed mice of the indicated genotype, L=lipid droplets, M=mitochondria, N=nucleus. B) Liver triglyceride concentrations are reduced in the mINDY$^{-/-}$ mice after a 6 week HFD (n=8). C) Hepatic membrane protein kinase ε content is reduced in mINDY$^{-/-}$ mice (n=4) D) Hepatic diacylglycerol (DAG), and ceramide concentrations as assessed by GC/MS/MS (n=7-8), all error bars represent SEM.

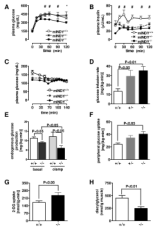

Figure 5.

In vivo glucose metabolism in mINDY mice after a 6 week HFD. A) Venous glucose concentrations during an intraperitoneal glucose tolerance test (IPGTT, 1mg/kg BW glucose) in overnight fasted mice of the indicated genotype (n=7-8). B) Venous insulin concentrations during the IPGTT (n=7-8). C) Plasma glucose concentrations during hyperinsulinemic-euglycemic clamp studies (n=7-8). D) Glucose infusion rate during hyperinsulinemic-euglycemic clamp studies is increased with deletion of *mIndy* (n=6-9). E) Endogenous glucose production in the basal and the clamped state (n=6-9). F) Peripheral glucose uptake during the hyperinsulinemic-euglycemic clamp studies (n=6-9). G) ^{14}C-2-deoxyglucose uptake into gastrocnemius muscle during the hyperinsulinemic-euglycemic clamp is increased with deletion of *mIndy* (n=5) H) Gastrocnemius muscle diacylglycerol (DAG) content assessed by LC/MS/MS is reduced in mINDY$^{-/-}$ mice (n=5). *P<0.05, #P<0.01 by two way ANOVA, all error bars represent SEM, also see Table S3.

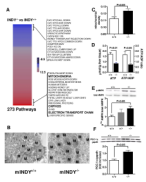

Figure 6.

Loss of *mIndy* enhances mitochondrial metabolism. A) Hepatic gene set enrichment analysis in young mINDY$^{-/-}$ mice compared to young mINDY$^{+/+}$ mice on a regular chow (n=4-5). B) Representative hepatic mitochondria (M) with similar EM-magnification. C) Mitochondrial density (mitochondrial number/counted cell volume) as assessed by the point counting method by a sample-blinded specialist using electron microscope magnification in liver slices of the indicated phenotype (n=3) D) Hepatic ATP content (left) and ATP/ADP ratio assessed with ^{31}P-MRS after a 24hr fast are reduced in mINDY$^{-/-}$ mice (n=5) E) Representative immunoblots of hepatic AMP activated protein kinase (AMPK) alpha Thr172 phosphorylation/ total AMPK content (n=6). F) Representative immunoblots of hepatic PGC-1α expression (n=6), all error bars represent SEM, see also Figure S5

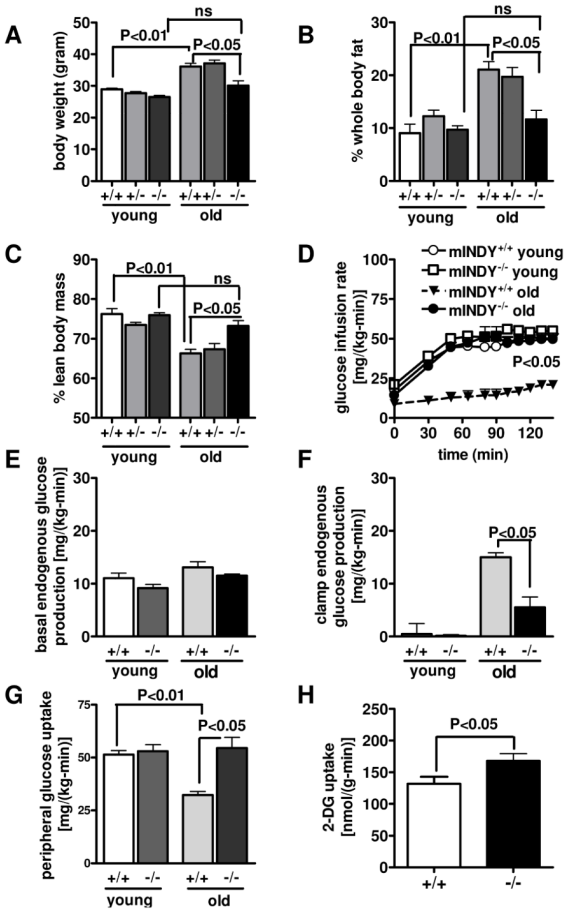

Figure 7.

Older mINDY mice are protected from adiposity and insulin resistance. A) Body weight in two-month old (young) and eight-month old mice (old) of the indicated phenotype (n=5-8). B) Proportion of whole body fat to body weight as assessed by ^{1}H magnetic resonance spectroscopy in two-month old (young) and eight-month old mice (old) of the indicated phenotype (n=5-8). The percentage of whole body fat did not change significantly in young compared to old mINDY$^{-/-}$ mice. C) Proportion of total lean body mass as assessed by ^{1}H magnetic resonance spectroscopy in two-month old (young) and eight-month old mice (old) of the indicated genotype (n=5-8). D) Glucose infusion rate during the hyperinsulinemic euglycemic clamp study in three-month old (young) and eight-month old (old) mice of the indicated genotype (n=5-8). Older mINDY$^{-/-}$ were protected from aging related insulin resistance. E) Basal endogenous glucose production in three-month old (young) and eight-month old (old) mice of the indicated genotype (n=6-7). F) Clamp endogenous glucose production in three-month old (young) and eight-month old (old) mice of the indicated genotype (n=6-7). G) Peripheral glucose uptake during the hyperinsulinemic-euglycemic clamp study in three-month old (young) and eight-month old (old) mice of the indicated genotype (n=6-7). H) ^{14}C-2-deoxyglucose uptake into gastrocnemius muscle during the hyperinsulinemic-euglycemic clamp studies in eight-month old mINDY$^{+/+}$ and mINDY$^{-/-}$ mice (n=6-7), all error bars represent SEM, ns=not significant.